Neurocomputing 149 (2015) 1560–1572

Contents lists available at ScienceDirect

Neurocomputing

journal homepage: www.elsevier.com/locate/neucom

Improved texture image classification through the use of a corrosion-inspired cellular automaton

Núbia Rosa da Silva [b,a], Pieter Van der Weeën [c], Bernard De Baets [c], Odemir Martinez Bruno [a,b,*]

[a] Scientific Computing Group, São Carlos Institute of Physics, University of São Paulo (USP), cx 369 13560-970 São Carlos, São Paulo, Brazil
[b] Institute of Mathematics and Computer Science, University of São Paulo (USP), Avenida Trabalhador são-carlense, 400, 13566-590 São Carlos, São Paulo, Brazil
[c] Department of Mathematical Modelling, Statistics and Bioinformatics, Ghent University, Coupure links 653, 9000 Ghent, Belgium

ARTICLE INFO

Article history:
Received 26 October 2013
Received in revised form
2 July 2014
Accepted 14 August 2014
Communicated by Xiaoqin Zhang
Available online 23 August 2014

Keywords:
Pattern recognition
Pitting corrosion
Texture classification
Cellular automata

ABSTRACT

In this paper, the problem of classifying synthetic and natural texture images is addressed. To tackle this problem, an innovative method is proposed that combines concepts from corrosion modeling and cellular automata to generate a texture descriptor. The core processes of metal (pitting) corrosion are identified and applied to texture images by incorporating the basic mechanisms of corrosion in the transition function of the cellular automaton. The surface morphology of the image is analyzed before and during the application of the transition function of the cellular automaton. In each iteration the cumulative mass of corroded product is obtained to construct each of the attributes of the texture descriptor. In the final step, this texture descriptor is used for image classification by applying Linear Discriminant Analysis. The method was tested on the well-known Brodatz and Vistex databases. In addition, in order to verify the robustness of the method, its invariance to noise and rotation was tested. To that end, different variants of the original two databases were obtained through addition of noise to and rotation of the images. The results showed that the proposed texture descriptor is effective for texture classification according to the high success rates obtained in all cases. This indicates the potential of employing methods taking inspiration from natural phenomena in other fields.

1. Introduction

The classification of texture images is an important problem in pattern recognition and consequently forms the subject of many research works in this field. Texture is an important image feature with a strong discriminative capability and is therefore widely used in computer vision. Image descriptors for image texture are obtained from the analysis of groups of pixels and the way this analysis is performed is used to classify the different methods of texture analysis. Based on the domain from which the texture feature is extracted, five main categories can be distinguished: structural [1–3], statistical [4], model-based [5–7], spectral [8,9], and agent-based methods [10–12].

This paper proposes a novel texture descriptor constructed by means of a cellular automaton (CA) taking inspiration from the pitting corrosion phenomenon, further on referred to as the Corrosion-Inspired Texture Analysis (CITA) descriptor. The basic mechanisms behind this detrimental reaction which occurs between metals (or alloys) and their environment serve as inspiration to develop a CA-based model. Next, this CA-based model is employed to generate a texture descriptor for classification by treating the image to be classified as a metal surface. The CA-based model, like real corrosion, amplifies existing differences in material and height (in this case grayscale value) so that the biggest contrasts in the original texture image will become more pronounced and smaller contrasts will be nullified. The eroded mass of 'metal' by the progression of pitting corrosion at each iteration is used to generate a texture descriptor that describes the image to be classified. These texture descriptors are then used as feature vectors in a supervised setting to develop a classification method. The effectiveness of this strategy is demonstrated on two texture databases, Brodatz and Vistex, with natural and synthetic textures. In addition, to verify the robustness of the classification method, its invariance to noise and rotation were tested, obtaining satisfactory results.

The main contribution of this work thus lies in demonstrating that a natural phenomenon can be a source of inspiration to develop a

* Corresponding author.
URLS: http://www.scg.ifsc.usp.br (N.R. da Silva), http://www.scg.ifsc.usp.br (O.M. Bruno).

http://dx.doi.org/10.1016/j.neucom.2014.08.036
0925-2312/

robust texture descriptor for the classification of both natural and synthetic texture images. Moreover, the proposed method outperforms the state-of-the-art methods in texture analysis, thus contributing to the image analysis field. Our paper is organized as follows. Section 2 describes the basics behind the pitting corrosion phenomenon, while the definition of a CA as well as further explanation of some parts of this definition form the subject of Section 3. The classification method is described in Section 4 and the experimental setup needed to test its efficacy is explained in Section 5. Section 6 presents the results and Section 7 presents the discussion of the study. Finally, the paper is concluded in Section 8.

2. Pitting corrosion

Corrosion is the disintegration of metals (and alloys) into their constituents due to reaction with the environment and is one of the main causes of structural failure in industrial systems, and poses as such an economic problem [13]. Dealing with corrosion is difficult because of its complex nature and the involvement of many variables. Therefore, modeling and simulation could allow for predicting more accurately the corrosion process in time. CA-based models are excellent candidates for modeling corrosion due to their intrinsic simplicity and therefore, since the beginning of the new millennium, attempts are being made to employ these models in the field of corrosion engineering [14–18]. Corrosion is present in a wide range of metals and environments, which points to the universality of this phenomenon. The latter suggests that corrosion does not depend on the details of the underlying mechanism, so that it may be modeled adequately using simple models [19]. Moreover, CA-based models are able to capture the stochasticity of the involved electrochemical reactions at the mesoscopic scale [16].

Pitting corrosion is a very harmful and common form of localized corrosion where all or most of the metal loss occurs concentrated in certain areas. Upon close inspection of the metal surface, pitting can be recognized by the appearance of small holes on the metal surface as shown in Fig. 1. The first step in pitting corrosion is the pit initiation which is the result of impurities or irregularities of the metal surface or the environment, making perfectly polished surfaces more resistant to this type of corrosion. From there on, the acidity inside the pit is maintained by the spatial separation of the cathodic and anodic half-reactions, which creates a potential gradient and electromigration of aggressive anions into the pit (see Fig. 1). As pit growth progresses, different solution compositions develop inside the cavity and the consequent voltage (IR) drop along the metal/electrolyte interface illustrates that the deeper the pit, the lower the pit growth rate [17,21,22].

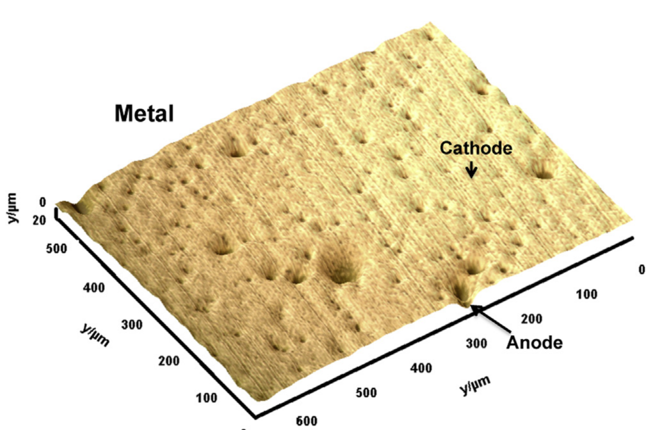

Fig. 1. Pitting corrosion: schematic representation in a metal surface.

3. Cellular automata

CAs are mathematical constructs in which the space, state and time domains are discrete as opposed to partial differential equations (PDE) in which these three domains are continuous [23,24]. The ability of CAs to generate a rich spectrum of sometimes complex spatio-temporal patterns from relatively simple underlying transition functions has led to their successful employment in the modelling of several biological processes [25–30]. Models based on CAs can be seen as an alternative to PDE-based models, to provide researchers with a wider range of modeling tools and, in some complex cases, a solution to problems encountered with some of the more classical modeling methods [31,32].

In this paper, we make use of a homogeneous CA, in which a single transition function, constructed using a combination of knowledge on the pitting corrosion phenomenon and intuition, governs the dynamics of all cells. The following definition of a homogeneous 2D CA is relied upon.

Definition 1 (*Homogeneous 2D cellular automaton*). A homogeneous 2D cellular automaton $\mathcal{C}$ can be represented as

$\mathcal{C} = \langle \mathcal{T}, S, s, N, \Phi \rangle$,

where

(i) $\mathcal{T}$ is a two-dimensional grid of cells c.
(ii) S is a finite set of k states, with $S \subset \mathbb{N}$.
(iii) The output function s yields the state $s(c,t)$ of every cell c at the t-th discrete time step.
(iv) The neighborhood function N determines the neighboring cells of every cell c, including the cell c itself.
(v) The transition function Φ yields the state $s(c,t+1)$ of every cell c at the next time step, based on its state and that of its neighboring cells at the current time step.

For reasons of comprehensiveness, some parts of this definition will be elaborated in the remainder of this section.

3.1. Grid $\mathcal{T}$

In this paper, a finite two-dimensional grid consisting of squares is used, because it has the most straightforward implementation and provides an easy way of linking the cells of $\mathcal{T}$ to the pixels of the texture images to be classified (cfr. infra). Furthermore, an indexing of the cells of a 2D CA is introduced, which is shown in Fig. 2. For a square grid, it holds that $i^* = j^* = \sqrt{|\mathcal{T}|}$.

3.2. Neighborhood function N

Many different neighborhoods can be defined in 2D, the two most important ones being the Moore and the von Neumann neighborhood. The Moore neighborhood of a cell $c_{i,j}$ comprises those cells that share at least a vertex with $c_{i,j}$ (see Fig. 3(a)). The von Neumann neighborhood is a more restricted neighborhood in which only those cells that share an edge with $c_{i,j}$ are considered as neighbors (see Fig. 3(b)).

3.3. Discrete states

Every cell $c_{i,j}$ has one of the k discrete states comprised in the set S. The states of the cells $c_{i,j}$ of $\mathcal{T}$ at $t=0$, i.e. $s(c_{i,j},0)$, constitute the initial condition of $\mathcal{T}$. In this paper, the initial condition of $\mathcal{T}$ is determined by the grayscale value of the different pixels of the corresponding texture image (cfr. infra).

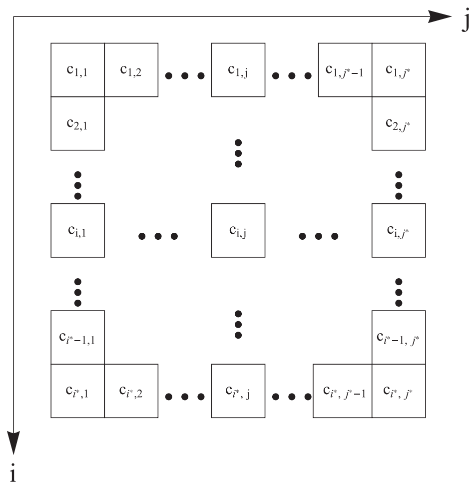

Fig. 2. Ordering of the cells of a 2D CA.

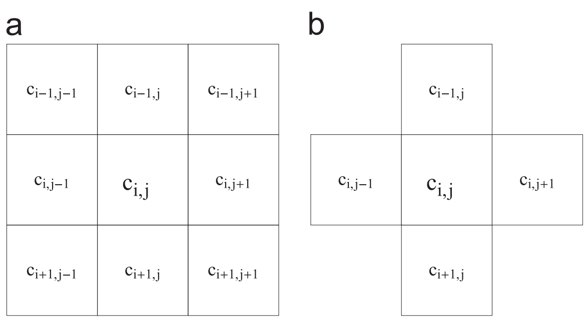

Fig. 3. Neighborhoods of a cell $c_{i,j}$ in a square tessellation: (a) Moore neighborhood and (b) von Neumann neighborhood.

3.4. Transition function Φ

The transition function Φ determines the state of a cell $c_{i,j}$ at the $(t+1)$-th time step based on the cell's current state and the states of its neighboring cells. The transition function employed in this paper is executed in a deterministic and synchronous manner, meaning that Φ is used to evaluate the state of every cell of $\mathcal{T}$ at every time step and for all cells at the same time [33].

4. Corrosion-inspired texture analysis

To obtain the texture descriptor proposed in this paper, initially, the texture image is converted into the initial state of a CA. Thereafter, a CA-based model inspired by the pitting corrosion phenomenon is evaluated for a number of time steps. The cumulative mass of corroded metal after each iteration of the CA-based model is used to construct a texture descriptor for every texture image. Finally, these texture descriptors are used to classify the images via Linear Discriminant Analysis (LDA). In the remainder of this section, the procedure to obtain the texture descriptor is explained in more detail.

A two-dimensional grayscale image is treated as a discrete object and is seen as a grid $\mathcal{T}$. The dimensions of $\mathcal{T}$ are defined by the size of the image, where each pixel of the image is a cell of the CA. The original image is then used to determine an initial state of the cells of the CA by converting the gray level image into a discrete initial state for each cell. Thus, for the initial configuration $s(c_{i,j},0)$ there are 256 possible states, ranging from 0 to 255. This conversion is described by

$$s(c_{i,j},0)=I(i,j), \tag{1}$$

where I is the original image and $I(i,j)$ represents the gray level of the pixel at the i-th row and j-th column of the image I. In order to introduce the ideas of pitting corrosion, the 2D grid will be regarded as a metal surface and the state of each cell will represent the depth of the local pit in the metal (i.e. along the third dimension), with state 0 meaning that there is no pit and 255 being the largest pit depth of the metal at $t=0$. It is important to point out that for $t>0$ the maximum pit depth can exceed 255 and from thereon it is possible that the grid can no longer be represented as a grayscale image.

An important consideration is the choice of boundary conditions in order to obtain an appropriate behavior of the CA-based model. The two most popular boundary conditions are the periodic and reflecting boundary conditions. The former tries to simulate an infinite grid, where the new boundaries of the top, bottom, left and right are filled with the values of the opposite side, thus forming a torus in a 3D space. This boundary condition is useful for simulating systems where the physical boundaries do not play an important role. However, throughout this paper, reflecting boundaries will be used as they give rise to better results for the studied databases as was observed from preliminary tests. Firstly, an imaginary row at the top and at the bottom of the grid and an imaginary column at the left and at the right of the grid are added. Then, the reflecting boundary conditions are applied at every time step as follows:

$$\begin{aligned}
&s(c_{1,j},t)=s(c_{2,j},t),\\
&s(c_{n+2,j},t)=s(c_{n+1,j},t),\\
&s(c_{i,1},t)=s(c_{i,2},t),\\
&s(c_{i,n+2},t)=s(c_{i,n+1},t),
\end{aligned} \tag{2}$$

with n the size of the original image with $n\times n$ pixels.

The updated state of each cell $c_{i,j}$ of $\mathcal{T}$ at time $t+1$ depends on the analysis of the states of the cells in the neighborhood of $c_{i,j}$ at time t. In this paper, the Moore neighborhood (see Fig. 3(a)) is employed. Furthermore, the CA-based model makes use of a transition function Φ taking inspiration from pitting corrosion. In a first step, $d_{i,j}$ is calculated for every cell $c_{i,j}$ as the difference between the state of this cell and the lowest state value within its Moore neighborhood (see the following equation):

$$d_{i,j}=s(c_{i,j},t)-\min(\tilde{s}(N(c_{i,j}),t)), \tag{3}$$

where $\tilde{s}(N(c_{i,j}),t)$ is the set of states of the cells in the Moore neighborhood of $c_{i,j}$.

Bearing in mind the principles of pitting corrosion, a local 'impurity' or minimum height difference is needed at a certain location in order to initiate or propagate pitting corrosion. For this purpose, a surface roughness parameter ν is introduced. All differences lower than this parameter ν are considered insignificant, i.e. not real impurities, in order to account for the fact that not even a polished metal surface is perfectly smooth. This means that differences $d_{i,j}$ lower than ν will not give rise to (further) pitting. On the other hand, the larger the difference grows, the lower the pit growth rate will be due to the IR drop, until finally the pit growth rate becomes zero. In this paper, it is assumed that if the difference $d_{i,j}$ is greater than 255, the greatest possible difference at $t=0$, the corresponding pit growth rate is zero. This means that only the state of those cells with a difference $d_{i,j}$ greater than or equal to ν and smaller than or equal to 255 are evaluated.

Fig. 4(a)–(c) illustrates the selection process to determine whether a cell will be evaluated or not. In this example, ν is set to five meaning that cells $c_{i,j}$ whose state differs less than five with the lowest state in its neighborhood are considered to belong to a

21	21	28	28	28
21	27	22	21	21
31	34	22	21	21
22	27	22	21	21
21	20	27	21	21

b

0	0	7	7	7
0	6	1	0	0
10	13	1	0	0
2	7	2	0	0
1	0	7	0	0

c

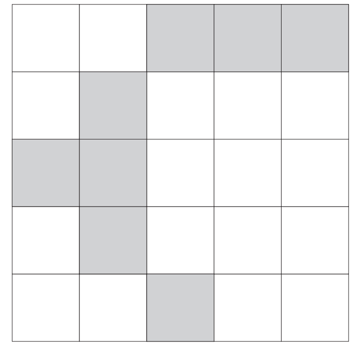

Fig. 4. Selection of cells to be updated, with $\nu=5$: (a) 5×5 square grid with initial states of the cells, (b) difference $d_{i,j}$ for all cells according to Eq. (3) and (c) gray cells indicate cells to be updated.

the surface and will not have their state changed. Fig. 4(a) shows the cells belonging to a 5×5 square tessellation with their initial state. Fig. 4(b) depicts the difference $d_{i,j}$ for each of these cells calculated according to Eq. (3). Finally, in Fig. 4(c) the gray cells indicate the cells that are evaluated in that time step, because their $d_{i,j}$ is greater than or equal to five and smaller than or equal to 255.

Under these assumptions, the transition function Φ establishes the state of a cell $c_{i,j}$ at the $(t+1)$-th time step according to

$$s(c_{i,j},t+1)=\begin{cases} s(c_{i,j},t)+Q(d_{i,j},\gamma) & \text{if } 255\geq d_{i,j}\geq\nu, \\ s(c_{i,j},t) & \text{if } d_{i,j}<\nu \text{ or } d_{i,j}>255, \end{cases} \tag{4}$$

where $\gamma\in[0,1]$ is the pitting power. This parameter γ represents the metal-specific resistance to corrosion under given environmental conditions, where $\gamma=0$ stands for completely resistant metal. Further, Q is a function that employs $d_{i,j}$ and γ to determine the level of corrosion to be applied. In this paper, Q is defined as

$$Q(d_{i,j},\gamma)=(255-d_{i,j})\gamma. \tag{5}$$

From Eq. (5), it can be seen that the function Q gives, depending on the value of γ, a non-integer output, meaning that the employed model structure is actually a continuous CA or Coupled Map Lattice rather than a CA [34]. However, in order to keep working with a CA-based model and to not overcomplicate the model, the choice was made to limit the output of Q to integer values (see the following equation):

$$Q(d_{i,j},\gamma)=\lfloor(255-d_{i,j})\gamma\rfloor, \tag{6}$$

where a in $\lfloor a\rfloor$ denotes the floor of a.

The output of the CA-based model at every time step is the cumulative mass of corroded product. In each iteration, after updating the state of the cells, the mass that suffered corrosion in that iteration is added to the eroded total mass from the previous iteration. Finally, this cumulative corroded mass is expressed relative to the number of pixels of the texture images such that texture images with different sizes can be compared. The time series of cumulative mass of corroded metal thus obtained will be used as texture descriptor for each image. The first column in Fig. 5 shows examples of some initial images, while the second and third columns show the simulated results after 90 iterations of the CA-based model, in grayscale and in a color map, respectively. Upon completion of the simulation, some structural details from the original image can still be retrieved in the simulated output. Regions with similar state values are mostly considered by the model as belonging to the same local surface and therefore tend to keep the same state value throughout the simulation.

The classification of the texture descriptors generated by the CA-based model is performed using LDA following a stratified 10-fold cross-validation scheme. The number of features is precisely the number of iterations of the CA-based model. LDA is traditionally used in texture analysis to find a linear combination of attributes resulting in a good separation of the classes. Although more sophisticated machine learning methods for classification exist, the intrinsic value of new features is best judged by means of a simple technique such as LDA. The procedure to obtain the proposed texture descriptor is summarized in Fig. 6. Fig. 7 shows the feature vectors for four texture images from the Brodatz database. It can be clearly seen from this figure that the feature vectors from textures belonging to the same class are very similar on one hand and that these vectors are different from the feature vectors from images belonging to different classes on the other hand.

5. Experimental setup

To investigate the performance of the classification method, it is employed for the classification of the images of two classical texture databases, the Brodatz and Vistex databases, and the results are compared to those obtained with several established features from the literature. The remainder of this section includes a short description of the employed databases and the features from the literature used for comparison as well as an optimization of the parameters of the procedure to obtain the CITA descriptor, i.e. γ, ν and the number of iterations performed in order to obtain the most favorable results. To ensure that the CITA descriptor is not sensitive to the parameter configuration, Usptex, a different database than the databases used for the validation of the method is used to perform the parameter optimization.

5.1. Databases

Two important databases, widely used in the literature and each with its own peculiarities, are employed for testing the different methods for pattern classification: the Brodatz and Vistex databases and a third database, Usptex, is used to perform the parameter optimization.

5.1.1. Brodatz database

The Brodatz database [35] contains 111 unique natural textures (and therefore also 111 classes) with image size of 640×640 pixels and 256 gray levels. From each image ten subimages with size of 200×200 pixels were obtained, resulting in an image database containing 1110 images. Fig. 8 shows the complete Brodatz database and Fig. 9(a) and (b) shows two original Brodatz images and ten subimages obtained from these original images without overlapping, respectively.

5.1.2. Vistex database

The Vistex database [36] contains 864 images belonging to 54 texture classes. Each texture class contains 16 texture samples of 128×128 pixels, each extracted from a particular texture pattern without overlapping (see Fig. 10). The true color RGB images are converted to grayscale intensity images, because the CITA descriptor in its present form is constructed making use of grayscale images.

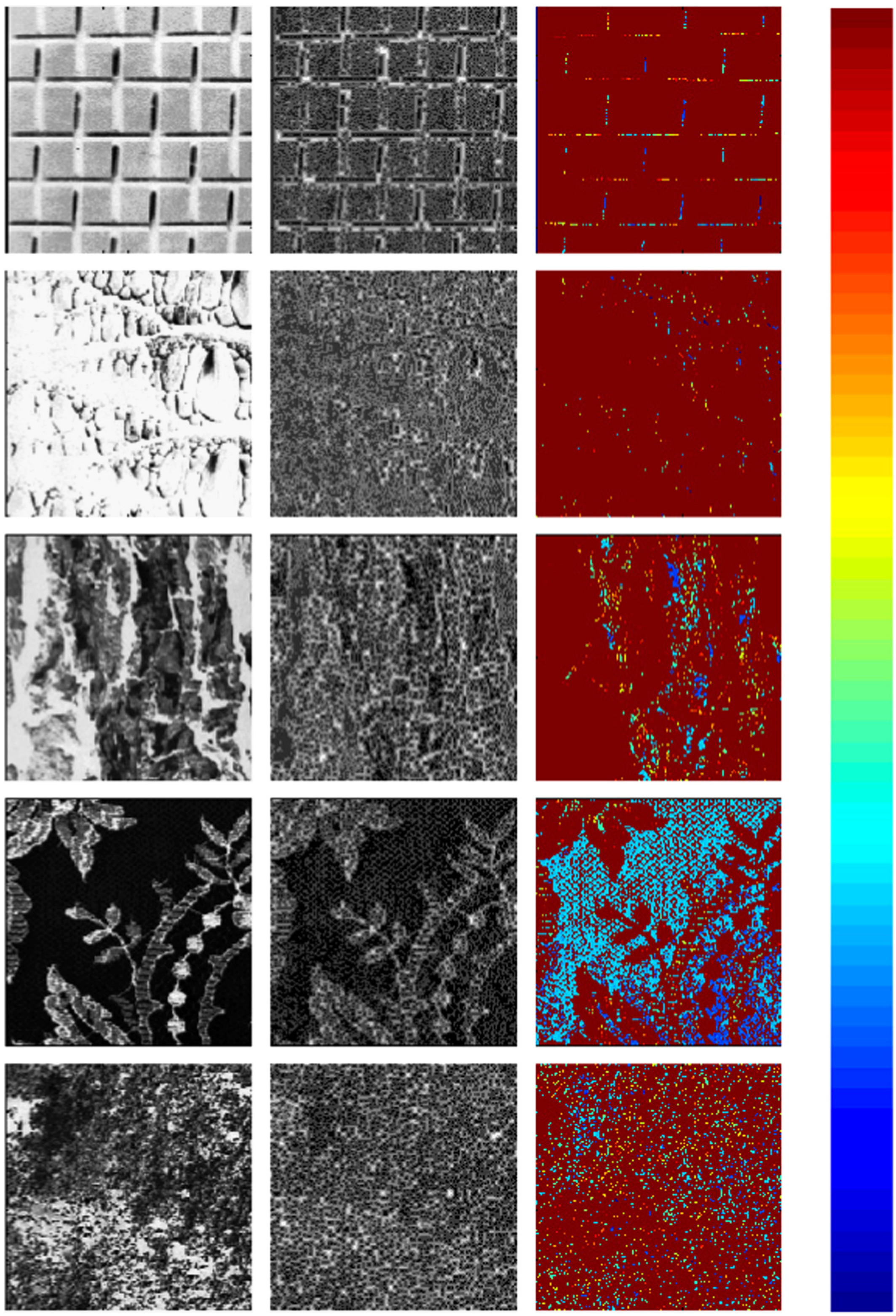

Fig. 5. Simulation results. First column: original images. Second column: result in grayscale after application of the CA-based model. Third column: result in blue-red scale after application of the CA-based model (see color code at the right hand side). The experiments were performed with $\gamma = 0.05$, $\nu = 5$ and 90 iterations. (For interpretation of the references to color in this figure caption, the reader is referred to the web version of this article.)

Input: Original image ($n \times n$), surface roughness ν, pitting power γ, number of iterations
Output: Class label

$s(c_{i,j}, 0) \leftarrow$ original image $(I(i,j))$

Add imaginary row at top and bottom
Add imaginary column at left and right

for all iterations **do**

    Apply boundary reflection on grid $\mathcal{T}$:

$$s(c_{1,j}, t) = s(c_{2,j}, t)$$
$$s(c_{n+2,j}, t) = s(c_{n+1,j}, t)$$
$$s(c_{i,1}, t) = s(c_{i,2}, t)$$
$$s(c_{i,n+2}, t) = s(c_{i,n+1}, t)$$

    for $i = 2 \to n+1$ **do**
        for $j = 2 \to n+1$ **do**
            $d_{i,j} \leftarrow s(c_{i,j}, t) - \min(\tilde{s}(N(c_{i,j}), t))$
            if $(d_{i,j} < \nu$ or $d_{i,j} \geq 255)$ **then**
                $s(c_{i,j}, t+1) \leftarrow s(c_{i,j}, t)$
            else
                $s(c_{i,j}, t+1) \leftarrow s(c_{i,j}, t) + Q(d_{i,j}, \gamma)$
            end if
        end for
    end for

    Calculate cumulative corroded mass

end for

Feature vector $\leftarrow$ cumulative corroded masses relative to number of pixels

Fig. 6. Pseudocode generating the CITA descriptor.

5.1.3. *Usptex database*

The Usptex database [37] contains 191 color images that each form a texture class (see Fig. 11). Each image has a size of 512×384 pixels from which 12 subimages with a size of 128×128 pixels are extracted without overlapping, so that a total of 2292 images is obtained. The images are again converted to grayscale images.

5.2. *Established features for texture analysis*

5.2.1. *Fourier descriptors*

Fourier descriptors [38,39] consider attributes in terms of spectral density considering the texture as a Gaussian random field. The Fourier transform was calculated for each image, where the spectrum was divided into 64 sectors with eight radial distances and eight angles. The sum of the absolute spectrum values for each sector is calculated, resulting in 64 descriptors per image.

5.2.2. *Gray level co-occurrence matrix*

The gray level co-occurrence matrix (GLCM) [4] is based on the spatial gray level dependence matrices. Haralick descriptors (contrast, correlation, energy and homogeneity) were computed from resulting co-occurrence matrices with angles of 0°, 45°, 90° and 135°, distances equal to one or two pixels and 64 gray levels in order to obtain a set of 32 descriptors for each image.

5.2.3. *Gray level difference matrix*

The gray level difference matrix (GLDM) [40,41] represents the absolute gray level difference between every two pixels with distance h. Here, 60 descriptors were obtained using $h=1$, 3 and

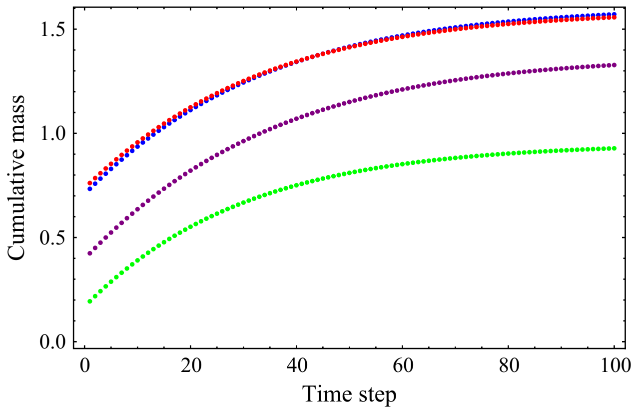

Fig. 7. Texture descriptor of four different texture images of the Brodatz database, with $\gamma=0.04$, $\nu=5$ and 100 iterations. The blue and red vectors originate from class 11 images, the purple vector from a class 24 image and the green vector from a class 78 image. (For interpretation of the references to color in this figure caption, the reader is referred to the web version of this article.)

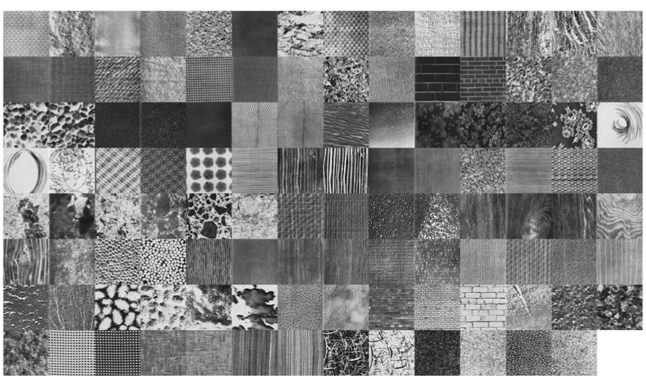

Fig. 8. The Brodatz database. The size of the images is 640×640 pixels.

5 and the attributes contrast, angular second moment, entropy, mean, and inverse difference moment from the estimated probability density function.

5.2.4. Gabor filter

A Gabor filter [42–44] is a bi-dimensional Gaussian function modulated with an oriented sinusoid in a determined frequency and direction. To perform the tests, 64 filters were used, composed of eight rotation filters and eight scale filters with lowest frequency equal to 0.01 and highest frequency equal to 0.4.

5.2.5. Local binary pattern variance

Local binary pattern variance (LBPV) [45] is a variation of traditional LBP [46] and is calculated from the binary value of each pixel in the radius 1 neighborhood surrounding the central pixel, measuring the local variance.

5.3. Parameter evaluation

In order to retrieve the parameters used in the procedure to obtain the CITA descriptor, the Usptex database, a different database than the ones used for validation is employed. This is done to ensure that the CITA descriptor is not susceptible to the parameters and therefore the same configuration can be used for classification of textures from different databases. The experiments in the remainder of this paper were performed using a stratified 10-fold cross-validation scheme [47] and LDA as classifier, both for the CITA descriptor as well as for the established features from literature.

5.3.1. Number of iterations

To describe each image, the cumulative mass of corroded metal after each iteration of the CA-based corrosion model is used. These values constitute the feature vector that is used to discriminate each of the images. However, finding a single number of iterations that gives rise to the smallest, most informative feature vector for all images of both databases is a non-trivial task due to the variety of the type of texture images and also because this number is dependent on the values of γ and ν. In order not to overcomplicate the problem, the choice is made to look for a single optimal number of iterations for the Usptex database that overall gives the best result for all the texture images. This optimal number of iterations is nevertheless still kept dependent on γ and ν.

5.3.2. Surface roughness ν

One of the parameters that defines the pitting corrosion is the surface roughness ν. According to the proposed corrosion-based method, pixels having a difference d lower than ν (Eqs. (3) and (4)) do not suffer from the action of the corrosion process, considering that they are part of the local surface. However, if the neighborhood has a difference d greater than the permitted threshold surface, the center pixel will pass through a corrosion process having its value eroded according to Eqs. (4) and (5). Fig. 12(a) shows the success rate surface, i.e. the percentage of correctly classified texture images, for the Usptex database for ν varying from 0 to 10 and γ varying from 0.01 to 0.08. The figure shows that higher values of ν lead to a lower success rate. However, when ν equals 0 the obtained success rate is smaller than for ν equal to 1 for almost all values of γ. Thus, a value of 1 for ν is chosen as optimal value.

5.3.3. Pitting power γ

Another model parameter with a physical meaning is the pitting power γ. This parameter is important because it determines the level of corrosion according to the material being eroded. However, as we are not dealing with real metal surfaces, this parameter is not known for the image texture analysis. Fig. 12(a) is now studied for γ ranging from 0.01 to 0.08. It can be seen that the highest success rate is obtained with γ and ν equal to 0.05 and 1, respectively. For values of γ below 0.05 the rate tends to be reduced while for values above 0.05 the rate also tends to decrease. When looking at combined high values of γ and ν the success rates drop sharply. Fig. 12(b) shows the number of iterations to obtain the highest success rate for each of the parameter combinations. The graph shows that the optimal number of iterations necessary for γ equal to 0.05 and ν equal to 1 is relatively low in comparison to the other results.

6. Results

This section reports on the performance of the proposed classification method. The classification performance when using the CITA descriptor is compared to that when using the traditional texture features in the literature. Three sets of experiments were performed: firstly on the original test databases and subsequently on modified versions of the test databases to test noise and rotation invariance. All tests were performed using the optimized values for ν, γ and the number of iterations identified in the previous section is shown in Table 1. For all experiments the success rate and the standard deviation (std) based on ten repetitions are shown for comparison of the results.

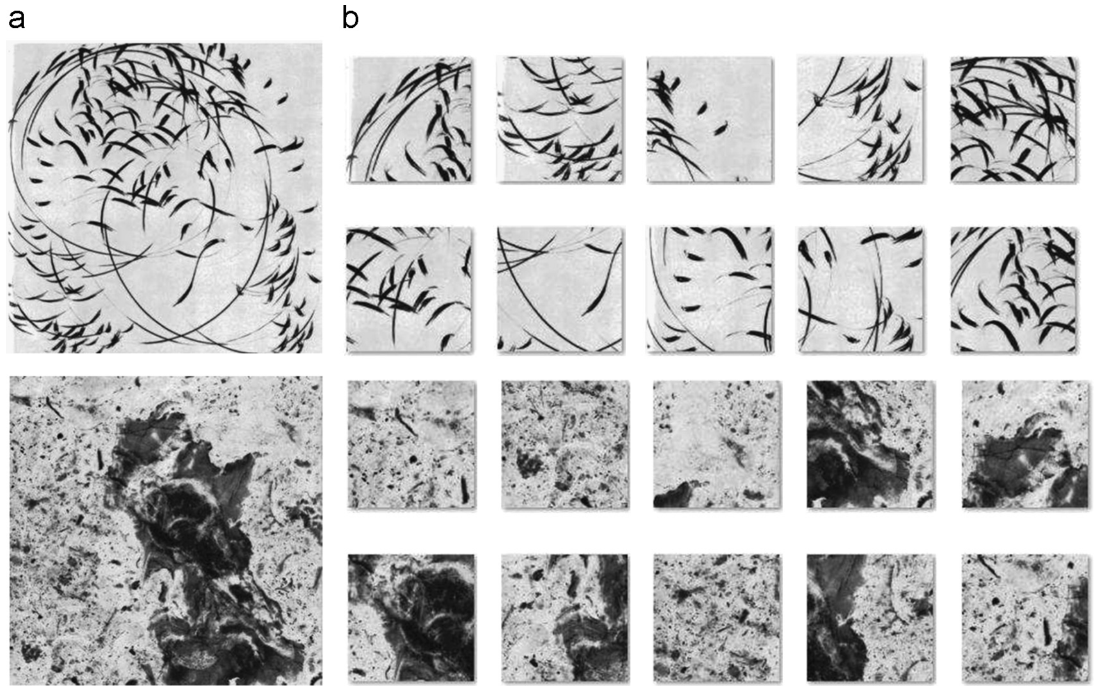

Fig. 9. (a) Two Brodatz textures of size 640 × 640 pixels and (b) ten subimages of size 200 × 200 pixels.

Fig. 10. The Vistex database. The size of the images is 128 × 128 pixels.

6.1. Unmodified databases

Table 2 lists the results obtained for the unmodified databases. As can be seen, an excellent success rate can be achieved by using the CITA descriptor, which is higher than the success rate for all other features for the Brodatz database and is of the same quality as the success rate obtained with GLDM for the Vistex database. To further test the robustness of the classification method based on the CITA descriptor, firstly, noise is applied to the images and, secondly, a rotation of the images is performed to verify whether the performance persists under these circumstances.

6.2. Noise invariance

In order to demonstrate the tolerance of the proposed classification method to noise, experiments were performed on modified versions of the Brodatz and Vistex databases with addition of noise in the form of ‘Salt and Pepper’ noise. By applying this type of noise to an image, black and white pixels are randomly added to the image matrix with an intensity l which may vary from 0 to 1 and represents the share of the image affected by the noise. The robustness of the classification method to the addition of noise is demonstrated by performing the texture classification on six modified databases generated from both the Brodatz and Vistex databases. The six different databases were generated in both cases by adding ‘Salt and Pepper’ noise with intensities $l = 0.01$,

Fig. 11. The Usptex database. The size of the images is 512 × 384 pixels.

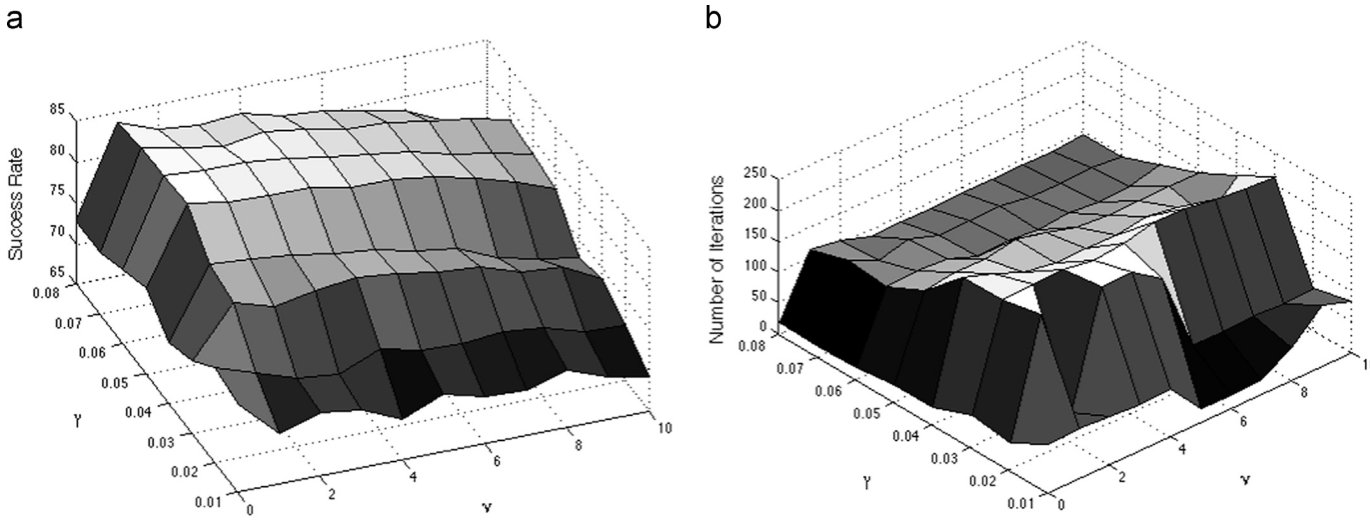

Fig. 12. (a) Pitting power and surface roughness analysis for the Usptex database with γ from 0.01 to 0.08 and ν from 0 to 10. (b) Number of iterations for each parameter configuration in (a).

Table 1
Optimal parameter values.

Parameter	Value
Number of iterations	158
ν	1
γ	0.05

Table 2
Comparison in terms of the success rate of texture classification making use of the CITA descriptor with classification making use of traditional texture analysis features for the unmodified databases.

Feature	Success rate (± std)	
	Brodatz	Vistex
Fourier	94 (± 2.4)	94 (± 1.9)
GLCM	94 (± 3.3)	94 (± 3.5)
GLDM	98 (± 0.9)	**97** (± 1.6)
Gabor filter	92 (± 3.7)	92 (± 1.7)
LBPV	88 (± 3.3)	82 (± 3.9)
CITA descriptor	**99** (± 1.5)	**97** (± 1.7)

0.05, 0.07, 0.1, 0.5 and 0.7. For all different cases the CITA descriptor is compared with the established features described in Section 5 in order to get an idea of how the CITA descriptor, in comparison with the other features, deals with deformation of texture. Fig. 13 shows samples of the modified Vistex databases where noise was added to the images and where each column shows examples of an intensity l of noise.

The success rates for classifying the perturbed images from the modified Brodatz and Vistex databases using the different features are given in Tables 3 and 4, respectively. These results were obtained with an addition of noise to both the training as well as the test data. Further, experiments using non-perturbated texture images for training and images with addition of noise for testing were performed. The results of the latter tests are shown in Tables 5 and 6.

6.3. Rotation invariance

The proposed CITA descriptor is intrinsically rotation invariant, and therefore good results are expected when tests are performed with modified databases with rotated images. To demonstrate the rotation invariance, additional versions of both the Brodatz and Vistex databases are created. Each image from the databases is rotated with the following angles: 0°, 45°, 90°, 135°, 180°, 225° and 270° and in this way, seven images are obtained from each original database image. Therefore, the new database with rotated Brodatz images has 70 images per class with 111 classes in total and the new database with rotated Vistex images has 112 images per class with 54 classes in total. Fig. 14 shows, for some texture images from the Brodatz database, the seven rotated images obtained under the different rotation angles, with all images on the same row originating from the same original image.

Table 7 shows the success rates for the classification of the texture images of the Brodatz and Vistex databases with rotated images. In this case, the success rates are obtained for the complete rotated Brodatz and Vistex databases, where each database consists of all rotated texture images of all the original images. The success rates achieved with the CITA descriptor are better than the success rates obtained with any of the other features and are comparable to the results obtained on the unmodified databases. These experimental results indicate that our descriptor has a good generalization ability. Hence, the descriptor described here has proven to be performant also for rotated texture classification.

7. Discussion

Our findings suggest that a CA-based model, taking inspiration from the natural phenomenon of pitting corrosion, results in informative features for subsequent texture classification. Experiments using the original Brodatz and Vistex databases have shown the capability of the CITA descriptor to discriminate between different textural classes. However, for the Vistex database, GLDM achieves the same success rate. The latter can be explained by the fact that, just like the CITA descriptor, GLDM uses differences in grayscale value between neighboring pixels to generate features. Nevertheless, the CITA descriptor has some distinctive characteristics. Firstly, it takes into account a larger neighborhood than GLDM and secondly, the CITA descriptor acquires additional information about the texture structure through its iterative nature. These characteristics can result in better texture classification, as shown for the original Brodatz database and for rotated textures, where the texture classification with the CITA descriptor

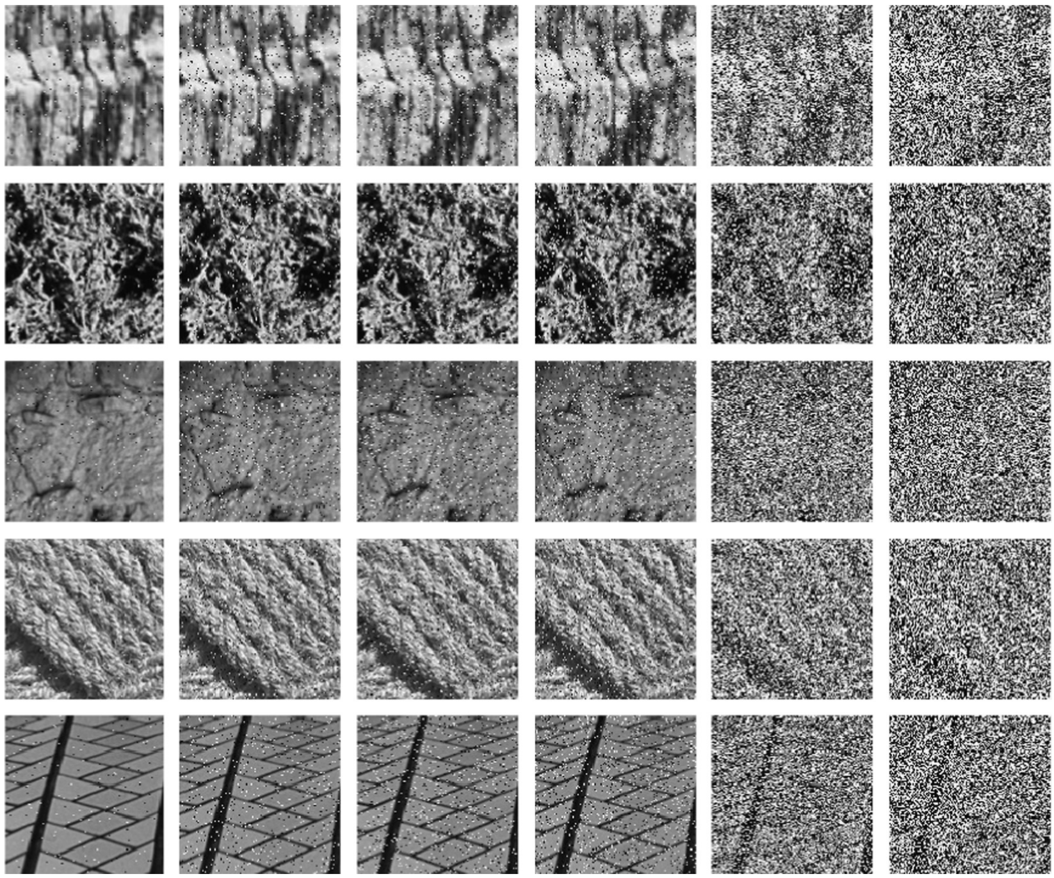

Fig. 13. Samples of six databases generated from the Vistex database by adding 'Salt and Pepper' noise. Each column represents an intensity of noise with $l=0.01$, 0.05, 0.07, 0.1, 0.5 and 0.7 from left to the right.

Table 3
Success rates of texture classification for six databases obtained through addition of different intensities l of 'Salt and Pepper' noise to the Brodatz database.

Feature	Success rate (± std)					
	$l=0.01$	$l=0.05$	$l=0.07$	$l=0.1$	$l=0.5$	$l=0.7$
Fourier	93 (± 2.6)	93 (± 3.3)	91 (± 3.5)	90 (± 3.5)	82 (± 4.9)	67 (± 6.1)
GLCM	94 (± 3.4)	94 (± 2.7)	95 (± 2.7)	94 (± 3.0)	87 (± 4.8)	76 (± 6.3)
GLDM	98 (± 1.5)	98 (± 1.5)	98 (± 1.5)	98 (± 1.8)	95 (± 2.1)	91 (± 3.5)
Gabor filter	91 (± 3.7)	90 (± 4.6)	90 (± 4.7)	90 (± 5.1)	82 (± 5.8)	67 (± 3.8)
LBPV	88 (± 3.1)	87 (± 3.8)	87 (± 4.5)	87 (± 4.8)	66 (± 5.2)	46 (± 6.4)
CITA descriptor	**99** (± 1.6)	**98** (± 1.3)	**98** (± 1.4)	**98** (± 1.2)	**97** (± 2.3)	**97** (± 1.7)

Table 4
Success rates of texture classification for six databases obtained through addition of different intensities l of 'Salt and Pepper' noise to the Vistex database.

Feature	Success rate (± std)					
	$l=0.01$	$l=0.05$	$l=0.07$	$l=0.1$	$l=0.5$	$l=0.7$
Fourier	93 (± 2.4)	91 (± 2.4)	89 (± 1.6)	89 (± 2.1)	67 (± 3.3)	35 (± 5.9)
GLCM	94 (± 2.9)	95 (± 1.6)	95 (± 2.8)	94 (± 1.8)	84 (± 3.8)	66 (± 4.3)
GLDM	**98** (± 1.1)	**97** (± 1.5)	**97** (± 1.8)	**97** (± 1.3)	**94** (± 1.4)	**86** (± 3.1)
Gabor filter	91 (± 2.2)	89 (± 1.7)	89 (± 3.2)	86 (± 3.2)	56 (± 5.9)	34 (± 3.9)
LBPV	83 (± 3.9)	83 (± 2.5)	82 (± 3.9)	81 (± 3.8)	54 (± 3.1)	39 (± 7.8)
CITA descriptor	96 (± 2.4)	94 (± 1.6)	94 (± 1.3)	94 (± 1.5)	**94** (± 4.7)	81 (± 4.5)

gives rise to a success rate that is 14% higher than the classification with GLDM for both the Brodatz and the Vistex databases.

Experiments to validate the noise invariance were performed by creating six new databases by adding 'Salt and Pepper' noise with different intensities to every image. The results demonstrate the good performance of our descriptor even with the addition of various intensities of noise. For all databases generated from Brodatz database, the classification with the CITA descriptor

Table 5
Success rates of classification of the texture images of the Brodatz database, with training data without addition of noise and test data with addition of different intensities l of 'Salt and Pepper' noise.

Feature	Success rate ($\pm$std)					
	l=0.01	l=0.05	l=0.07	l=0.1	l=0.5	l=0.7
Fourier	90 ($\pm$2.6)	**62** ($\pm$3.5)	**50** ($\pm$4.0)	**36** ($\pm$2.6)	4 ($\pm$0.9)	1 ($\pm$1.2)
GLCM	49 ($\pm$2.1)	6 ($\pm$0.9)	4 ($\pm$0.5)	3 ($\pm$0.7)	1 ($\pm$0.0)	1 ($\pm$0.0)
GLDM	84 ($\pm$5.2)	42 ($\pm$3.0)	16 ($\pm$1.6)	9 ($\pm$0.6)	1 ($\pm$0.0)	1 ($\pm$0.0)
Gabor filter	73 ($\pm$4.9)	57 ($\pm$1.9)	32 ($\pm$1.5)	26 ($\pm$2.2)	**7** ($\pm$1.1)	4 ($\pm$0.8)
LBPV	57 ($\pm$3.3)	14 ($\pm$1.3)	10 ($\pm$1.4)	9 ($\pm$0.7)	1 ($\pm$0.0)	1 ($\pm$0.0)
CITA descriptor	**97** ($\pm$2.8)	37 ($\pm$3.4)	20 ($\pm$1.7)	11 ($\pm$1.4)	6 ($\pm$1.9)	**4** ($\pm$0.8)

Table 6
Success rates of classification of the texture images of the Vistex database, with training data without addition of noise and test data with addition of different intensities l of 'Salt and Pepper' noise.

Feature	Success rate ($\pm$std)					
	l=0.01	l=0.05	l=0.07	l=0.1	l=0.5	l=0.7
Fourier	58 ($\pm$4.3)	10 ($\pm$2.1)	8 ($\pm$2.1)	6 ($\pm$2.1)	3 ($\pm$1.1)	2.1 ($\pm$1.1)
GLCM	64 ($\pm$3.6)	**33** ($\pm$1.4)	5 ($\pm$0.6)	2 ($\pm$0.6)	2 ($\pm$0.6)	2 ($\pm$0.6)
GLDM	**90** ($\pm$2.6)	13 ($\pm$1.4)	13 ($\pm$1.1)	9 ($\pm$1.3)	2 ($\pm$0.6)	2.3 ($\pm$1.1)
Gabor filter	58 ($\pm$2.8)	14 ($\pm$3.4)	10 ($\pm$2.2)	5. ($\pm$1.6)	2 ($\pm$0.6)	2 ($\pm$0.6)
LBPV	52 ($\pm$2.7)	14 ($\pm$2.7)	7 ($\pm$1.6)	5.6 ($\pm$1.6)	2 ($\pm$0.6)	2 ($\pm$0.6)
CITA descriptor	83 ($\pm$3.4)	23 ($\pm$4.3)	**17** ($\pm$2.6)	**11** ($\pm$1.7)	**6** ($\pm$3.3)	**5** ($\pm$2.9)

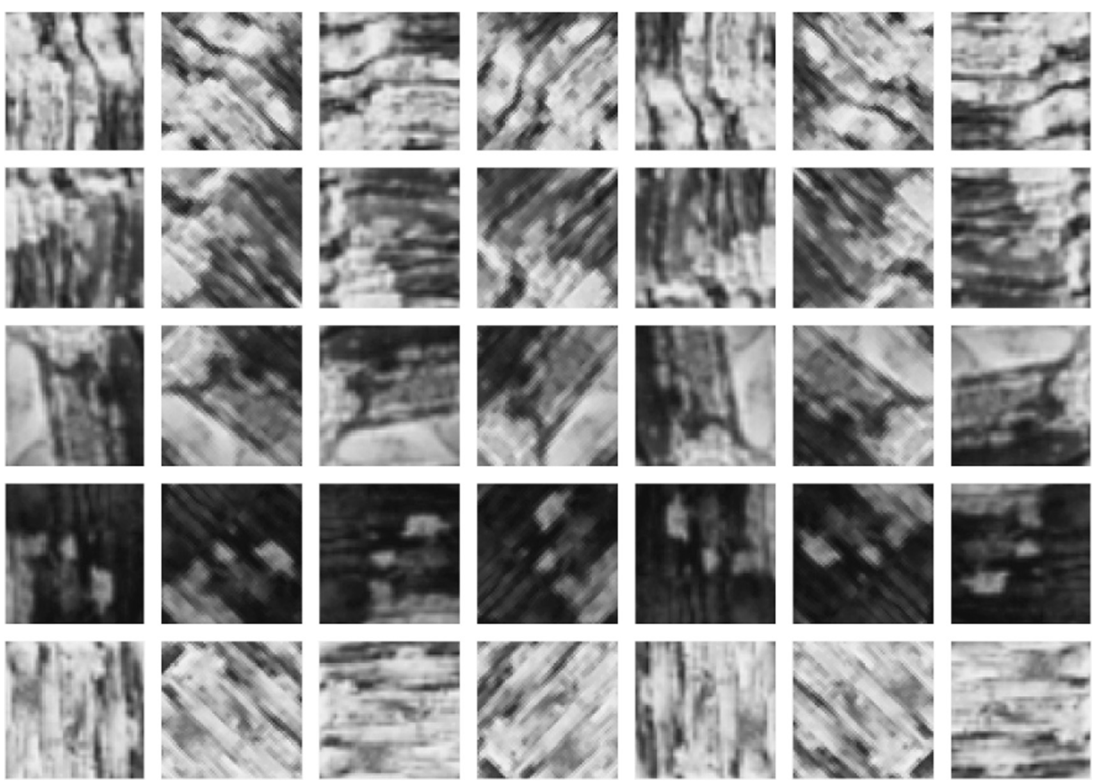

Fig. 14. Samples of rotated images from the Brodatz database. Each column corresponds to a different rotation angle. From left to right: 0°, 45°, 90°, 135°, 180°, 225° and 270°.

results in a higher success rate compared to traditional features in literature. It is important to note that even with increasing noise levels, the classification with the CITA descriptor yields high success rates, while for classification with all other features the success rate declines. For the databases generated from Vistex database, texture classification making use of our descriptor gives rise to the second best success rate, preceded by classification with GLDM, but still demonstrating its robustness to noise.

The best results are not achieved making use of the CITA descriptor compared to the other features considered in this paper when the images with addition of noise are only used as test data, while employing the original texture images as training data. However, the success rates obtained for classification with the CITA descriptor are comparable to those obtained for classification with the other features for both the Brodatz and Vistex databases. The use of the proposed CITA descriptor for classification does not

Table 7
Comparison in terms of the success rate of texture classification making use of the CITA descriptor with classification making use of traditional texture analysis features for the databases of rotated images.

Feature	Success rate (± std)	
	Rotated Brodatz	Rotated Vistex
Fourier	83 (± 1.1)	77 (± 1.3)
GLCM	71 (± 0.6)	74 (± 1.3)
GLDM	84 (± 0.5)	83 (± 0.7)
Gabor filter	78 (± 0.9)	71 (± 1.3)
LBPV	63 (± 1.0)	62 (± 1.7)
CITA descriptor	**98** (± 0.4)	**97** (± 0.7)

always result in the highest success rates for the different noise intensities and the two databases, nor is it the worst feature in any of the studied cases.

8. Conclusions

In this paper, a new descriptor for texture analysis was proposed by combining concepts from corrosion engineering, cellular automata and pattern recognition. The developed CITA descriptor in combination with LDA was used to classify the texture images of two well-known databases: Brodatz and Vistex. The descriptor was derived from images of the original databases and the robustness of the classification method under addition of noise and rotation was investigated. For this purpose, several new databases were created, starting from the original databases. Six new databases were obtained by adding 'Salt and Pepper' noise with different intensities to each of the images of the test databases and another new database was obtained by rotating the images of the databases under seven angles. In all cases, the texture classification making use of the CITA descriptor obtained good results compared to the classification making use of features from the literature, showing a good generalization ability and proving to be performant for texture classification.

The results presented in this paper demonstrate the potential of the CITA descriptor. Therefore, future work should focus on further refining the feature generation procedure as well as expanding it so that it is applicable for more types of texture images. This can be done by integrating measures of corrosion frequency via a histogram of eroded pixels and measuring the velocity of corrosion by calculating the difference between initial and final values divided by the number of iterations. Further, the procedure to generate the CITA descriptor has to be expanded so that it can deal with RGB color images as well as with dynamic textures, i.e. sequences of images that together form a texture.

Acknowledgments

Núbia Rosa da Silva acknowledges support from FAPESP (The State of São Paulo Research Foundation), Grant no. 2011/21467-9. Pieter Van der Weeën was sponsored by the Fund for Scientific Research in Flanders (FWO). Odemir Martinez Bruno gratefully acknowledges the financial support of CNPq (National Council for Scientific and Technological Development, Brazil) (Grant nos. 308449/2010-0 and 473893/2010-0) and FAPESP (Grant no. 2011/01523-1).

References

[1] R. Goyal, W. Goh, D. Mital, K. Chan, Scale and rotation invariant texture analysis based on structural property, in: Proceedings of the 1995 IEEE IECON 21st International Conference on Industrial Electronics, Control, and Instrumentation, vol. 2, pp. 1290–1294.
[2] J. Serra, Image Analysis and Mathematical Morphology, Academic Press, Inc., Orlando, FL, USA, 1983.
[3] J. Zhang, T. Tan, Brief review of invariant texture analysis methods, Pattern Recognit. 35 (2002) 735–747.
[4] R.M. Haralick, Statistical and structural approaches to texture, Proc. IEEE 67 (1979) 786–804.
[5] A.R. Backes, D. Casanova, O.M. Bruno, Plant leaf identification based on volumetric fractal dimension, Int. J. Pattern Recognit. Artif. Intell. 23 (2009) 1145–1160.
[6] A.R. Backes, O.M. Bruno, A new approach to estimate fractal dimension of texture images, in: A. Elmoataz, O. Lezoray, F. Nouboud, D. Mammass (Eds.), Image and Signal Processing, Lecture Notes in Computer Science, vol. 5099, Springer Berlin/Heidelberg, 2008, pp. 136–143.
[7] F. Cohen, Z. Fan, M. Patel, Classification of rotated and scaled textured images using Gaussian Markov random field models, IEEE Trans. Pattern Anal. Mach. Intell. 13 (1991) 192–202.
[8] C. Chen, A Comparative Study of Texture Classification Using Spectral Features, Technical Report ADA109408, pp. 1074–1077.
[9] X. Tang, W. Stewart, Texture classification using wavelet packet and Fourier transforms, in: Proceedings of Challenges of Our Changing Global Environment (OCEANS '95), MTS/IEEE, vol. 1, pp. 387–396.
[10] A.R. Backes, W.N. Gonçalves, A.S. Martinez, O.M. Bruno, Texture analysis and classification using deterministic tourist walk, Pattern Recognit. 43 (2010) 685–694.
[11] A.R. Backes, A.S. Martinez, O.M. Bruno, Color texture analysis and classification: an agent approach based on partially self-avoiding deterministic walks, in: Proceedings of the 15th Iberoamerican Congress Conference on Progress in Pattern Recognition, Image Analysis, Computer Vision, and Applications (CIARP'10), Springer-Verlag, Berlin, Heidelberg, 2010, pp. 6–13.
[12] M.-S. Lai, H.-C. Huang, S.-C. Chu, Image texture segmentation with ant colony systems, in: Proceedings of the First International Conference on Innovative Computing, Information and Control (ICICIC '06), vol. 1, IEEE Computer Society, Washington, DC, USA, 2006, pp. 652–656.
[13] P.R. Roberge, Corrosion Engineering: Principles and Practice, McGraw-Hill Professional, 2008.
[14] G. Contreras, S. Goidanich, S. Maggi, C. Piccardi, M.V. Diamanti, M.P. Pedeferri, L. Lazzari, Representing localized corrosion processes through cellular automata, Corros. Rev. 29 (2011) 241–245.
[15] D. di Caprio, C. Vautrin-Ul, J. Stafiej, J. Saunier, A. Chaussé, D. Féron, J.P. Badiali, Morphology of corroded surfaces: contribution of cellular automaton modelling, Corros. Sci. 53 (2011) 418–425.
[16] S.V. Lishchuk, R. Akid, K. Worden, J. Michalski, A cellular automaton model for predicting intergranular corrosion, Corros. Sci. 53 (2011) 2518–2526.
[17] B. Malki, B. Baroux, Computer simulation of the corrosion pit growth, Corros. Sci. 47 (2005) 171–182.
[18] R.M. Pidaparti, M.J. Palakal, L. Fang, Cellular automata approach to aircraft corrosion growth, Int. J. Artif. Intell. Tools 14 (2005) 361–369.
[19] A. Valor, F. Caleyo, L. Alfonso, D. Rivas, J.M. Hallen, Stochastic modeling of pitting corrosion: a new model for initiation and growth of multiple corrosion pits, Corros. Sci. 49 (2007) 559–579.
[21] H.W. Pickering, The significance of the local electrode potential within pits, crevices and cracks, Corros. Sci. 29 (1989) 325–341.
[22] H. Wang, B. Song, L. Wang, G. Lv, Three dimensional cellular automaton for simulation of the multi-pi corrosion damage evolution, Adv. Sci. Lett. 4 (2011) 2980–2985.
[23] L. Berec, Techniques of spatially explicit individual-based models: construction, simulation and mean-field analysis, Ecol. Model. 150 (2002) 55–81.
[24] S. Wolfram, Statistical mechanics of cellular automata, Rev. Mod. Phys. 55 (1983) 601–644.
[25] J. Milne, S.C. Fu, Epidemic modelling using cellular automata, in: Proceedings of the 1st Australian Conference on Artificial Life, pp. 43–57.
[26] C. Picioreanu, M. van Loosdrecht, J. Heijnen, Mathematical modelling of biofilm structure with a hybrid differential-discrete cellular automaton approach, Biotechnol. Bioeng. 58 (1998) 101–116.
[27] L. Preziosi, Modelling and Simulation, Chapman & Hall, Boca Raton, United States, 2003.
[28] J. Schiff, Cellular Automata: A Discrete View of the World, John Wiley & Sons Ltd., Chichester, United Kingdom, 2008.
[29] P. Van der Weeën, J.M. Baetens, J. Verwaeren, X. Van Doorslaer P.M. Heynderickx, J. Dewulf, B. De Baets, Modeling the photocatalytic degradation of moxifloxacin by means of a stochastic cellular automaton, Chem. Eng. J. 188 (2012) 181–190.
[30] Z. Vasilkoski, C.D. Weaver, A generator of protein folding kinetics states for the diffusion-collision model, J. Comput. Chem. 21 (2000) 923–932.
[31] S. El Yacoubi, A. El Jai, Cellular automata and spreadability, Math. Comput. Model. 36 (2002) 1059–1074.
[32] T. Toffoli, Cellular automata as an alternative to (rather than an approximation of) differential equations in modeling physics, Physica D 10 (1984) 117–127.

[33] J.M. Baetens, P. Van der Weeën, B. De Baets, Effects of asynchronous updating in cellular automata, Chaos, Solitons Fractals 45 (2012) 383–394.
[34] H. Levine, W.N. Reynolds, Coupled map lattice techniques for simulating interfacial phenomena in reaction-diffusion systems, Chaos 2 (1992) 337–342.
[35] P. Brodatz, Textures: A Photographic Album for Artists and Designers, Dover Publications, 1966.
[36] VisTex, Vision Texture Database, 2009.
[37] A.R. Backes, D. Casanova, O.M. Bruno, Color texture analysis based on fractal descriptors, Pattern Recognit. 45 (2012) 1984–1992.
[38] R. Azencott, J.-P. Wang, L. Younes, Texture classification using windowed Fourier filters, IEEE Trans. Pattern Anal. Mach. Intell. 19 (1997) 148–153.
[39] R.C. Gonzalez, R.E. Woods, Digital Image Processing, 3rd edition, Prentice-Hall, Inc., Upper Saddle River, NJ, USA, 2006.
[40] J.S. Weszka, C.R. Dyer, A. Rosenfeld, A comparative study of texture measures for terrain classification, IEEE Trans. Syst., Man Cybern. 6 (1976) 269–285.
[41] J.K. Kim, H.W. Park, Statistical textural features for detection of microcalcifications in digitized mammograms, IEEE Trans. Med. Imaging 18 (1999) 231–238.
[42] B. Manjunath, W. Ma, Texture features for browsing and retrieval of image data, IEEE Trans. Pattern Anal. Mach. Intell. 18 (1996) 837–842.
[43] J. Daugman, C. Downing, Gabor wavelets and statistical pattern recognition, in: M.A. Arbib (Ed.), The Handbook of Brain Theory and Neural Networks, MIT Press, Cambridge, MA, USA, 1998, pp. 414–420.
[44] M. Idrissa, M. Acheroy, Texture classification using Gabor filters, Pattern Recognit. Lett. 23 (2002) 1095–1102.
[45] Z. Guo, L. Zhang, D. Zhang, Rotation invariant texture classification using lbp variance (lbpv) with global matching, Pattern Recognit. 43 (2010) 706–719.
[46] T. Ojala, M. Pietikäinen, T. Mäenpää, Multiresolution gray-scale and rotation invariant texture classification with local binary patterns, IEEE Trans. Pattern Anal. Mach. Intell. 24 (2002) 971–987.
[47] T. Hastie, R. Tibshirani, J. Friedman, The elements of statistical learning, in: Springer Series in Statistics, Springer New York Inc., New York, NY, USA, 2001.

Núbia Rosa da Silva received the BA degree in Computer Science from Federal University of Goiás in 2007 and the M.Sc. degree in Computer Science from Federal University of Uberlândia in 2010. Now, she is a Ph.D. candidate in Computer Science at University of São Paulo. She joined the Scientific Computing Group in 2010 and her research interests include computer vision, image processing, and pattern recognition.

Pieter Van der Weeën (1987) holds an M.Sc. in Bioscience Engineering (2010), and a Ph.D. in Applied Biological Sciences (2014) both from Ghent University (Belgium).

Bernard De Baets (1966) holds an M.Sc. in Maths (1988), a Postgraduate degree in Knowledge Technology (1991) and a Ph.D. in Maths (1995), all summa cum laude from Ghent University (Belgium) and is a Government of Canada Award holder (1988). He is a Full Professor in Applied Maths (1999) at Ghent University, where he is leading KERMIT, the research unit Knowledge-Based Systems. He is an Honorary Professor of Budapest Tech (2006) and an IFSA Fellow (2011). His publications comprise more than 350 papers in international journals and about 60 book chapters. He serves on the Editorial Boards of various international journals, in particular as co-editor-in-chief of Fuzzy Sets and Systems. B. De Baets coordinates EUROFUSE, the EURO Working Group on Fuzzy Sets, and is a member of the Board of Directors of EUSFLAT and of the Administrative Board of the Belgian OR Society.

Odemir Martinez Bruno is an Associate Professor at the Physics Institute of S. Carlos at the University of S. Paulo in Brazil and head of the Scientific Computer Group. He received his B.Sc. in Computer Science (1992), from the Piracicaba Engineering College (Brazil), his M.Sc. in Applied physics (1995) and his Ph.D. in Computational Physics (2000) at the University of S. Paulo (Brazil). His fields of interest include Computer Vision, Image Analysis, Chaos, Fractals, Computational Physics, Pattern Recognition and Bioinformatics. He is an author of many papers (journal and proceedings) and several book chapters. He is a co-author of two books (Optical and Physiology of Vision: a multidisciplinary approach (Portuguese only) and Internet programming with PHP (Portuguese only)) and an inventor of seven patents.